# Land-Contamination Compensation for QuikSCAT Near-Coastal Wind Retrieval

Michael P. Owen and David G. Long, *Fellow, IEEE*

***Abstract*—The QuikSCAT scatterometer is used to accurately retrieve winds over the ocean at both high (2.5 km) and low (25 km) resolutions. In near-coastal regions, land contamination of measurements results in inaccurate wind estimates using current techniques. Here, we show that identifying land-contaminated measurements allows wind retrieval to be accurately achieved in near-coastal regions using QuikSCAT data at up to 2.5-km resolution using the AVE algorithm. To identify and remove land contamination, two metrics are compared, namely, the minimum distance to land and the land contribution ratio (LCR). The LCR is used as a metric to identify and remove land-contaminated backscatter $\sigma^o$ measurements before wind retrieval by discarding measurements with LCR values above a threshold. LCR thresholds used to remove land-contaminated measurements are determined using Monte Carlo simulations and set during processing using a lookup table based on the local wind speed, land brightness, and the cross-track swath location. Wind retrieval from $\sigma^o$ fields generated using the LCR is more accurate closer to the coast than previously achieved using both low- and high-resolution processing.**

***Index Terms*—Wind, scattering.**

## I. Introduction

THE SEAWINDS scatterometer was flown twice, once on the QuikSCAT platform and once on ADEOS II. The SeaWinds on QuikSCAT scatterometer, hereafter referred to as QuikSCAT, was launched in 1999. The QuikSCAT scatterometer offers invaluable analysis of winds over the ocean by providing daily coverage of nearly the entire Earth each day. QuikSCAT is not limited by cloud cover or light conditions. Although advantageous for those reasons, QuikSCAT is limited by measurement clutter in coastal regions [1]. Coastal winds are of particular interest due to their large economic and societal impact. Considering that the radar backscatter from land is much brighter than that from calm ocean water, there is significant contamination of the backscatter measurements, termed $\sigma^o$, near the coast due to antenna sidelobes. To facilitate accurate wind retrieval, land-contaminated $\sigma^o$ measurements must be identified and disregarded during wind retrieval. We propose an improved method to determine the impact of land contamination and discard contaminated measurements.

Manuscript received October 17, 2007; revised March 5, 2008.

The authors are with the Microwave Earth Remote Sensing Laboratory, Electrical and Computer Engineering Department, Brigham Young University, Provo, UT 84602 USA.

Color versions of one or more of the figures in this paper are available online at http://ieeexplore.ieee.org.

Digital Object Identifier 10.1109/TGRS.2008.2005633

In this paper, after a brief overview of QuikSCAT, we first evaluate two metrics for the detection of land-contaminated $\sigma^o$ measurements, namely, the minimum distance to land (MDL) and land contribution ratio (LCR). After comparing each metric, we simulate threshold levels for use in wind retrieval using the LCR. Finally, conventional (25 km) and high-resolution (2.5 km) [2] wind retrievals are performed using the LCR as the land-contamination metric for an illustrative region. We find that wind retrieval using the LCR effectively removes land contamination and allows wind retrieval up to 25 km closer to the coast than previously possible.

Section II gives an overview of relevant information on the SeaWinds scatterometer, Section III introduces and evaluates each land-contamination metric, Section IV discusses the creation of the LCR threshold lookup table, and Section V compares wind-retrieval results with and without LCR threshold processing.

## II. QuikSCAT Overview

Scatterometers are designed to obtain measurements of each wind vector cell (WVC) with a variety of azimuth angles to reduce directional ambiguity during wind retrieval. The QuikSCAT scatterometer measures backscatter values from the Earth's surface using both horizontally and vertically polarized microwave pulses at 13.4 GHz.

Using onboard range and Doppler processors, the backscatter value for each microwave pulse is separated into 12 regions. These regions are termed slices [3], each of which has a separate $\sigma^o$ value. Only 8–10 of the slices are used in processing, as the others have higher error and noise levels. The spatial response for each slice is known separately, and the individual response patterns are typically represented using the 3-dB contour for each response during resolution enhancement [4]. The 3-dB contours are roughly rectangular or oval with approximate dimensions of $30 \times 7$ km, where the longer dimension is termed the major axis and the shorter the minor axis [5]. Fig. 1 shows a contour plot of an example response function for a single slice with color contours spaced every 3 dB.

A recently developed resolution-enhancement algorithm [6] uses the $\sigma^o$ value and the 3-dB contour for each slice [4]. This resolution-enhancement algorithm was originally designed to use multiple passes of data to generate a higher resolution $\sigma^o$ field for each polarization and look (vertical, horizontal, fore, and aft). Multiple passes are inappropriate for wind retrieval due to the change in winds over time; thus, in this paper, we use the AVE algorithm [7]. The AVE algorithm is a single-pass form of the resolution-enhancement algorithm which creates high-resolution $\sigma^o$ fields prior to wind retrieval.

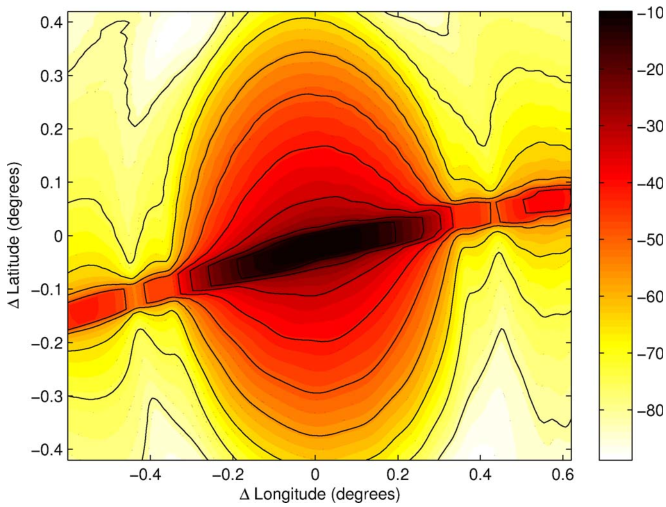


Fig. 1. Contours of the SeaWinds response function for a vertically polarized slice spaced every 10 dB. For this slice, the minor-axis direction is approximately up and down, and the major-axis direction is perpendicular. The background color contours are spaced every 3 dB. Note that the spatial response falls much faster in the minor-axis direction.

Fig. 2 shows the high-resolution $\sigma^o$ fields produced by the AVE algorithm for vertically polarized forward- and aft-looking measurements and the corresponding 3-dB contours. Land contamination of the $\sigma^o$ values is visually apparent in the way that the higher land $\sigma^o$ values spread away from the coastline. It is interesting to note that when the major axis is perpendicular to the coastline, the land contamination appears to reach further into the ocean than when the major axis is parallel to the coastline.

Land contamination of $\sigma^o$ measurements directly affects wind retrieval, which is the process of inferring the surface wind vector directly from the backscatter fields produced by the AVE algorithm. Wind retrieval is performed using a geophysical model function (GMF) which maps $\sigma^o$ measurements to wind vectors [8]. The GMF returns multiple possible wind vectors, known as ambiguities [9], for each WVC. Greater wind speeds are associated through the GMF with higher backscatter values. Land-contaminated $\sigma^o$ values are typically much higher than ocean $\sigma^o$ values [10] and thus appear as high wind speeds. When land-contaminated $\sigma^o$ values are used in wind retrieval, the speeds retrieved using the GMF are as much as 20 m/s higher than the true wind speed.

Once excessively land-contaminated $\sigma^o$ are identified and discarded, wind retrieval from valid $\sigma^o$ values can be done at either conventional or high-resolution. This results in uncontaminated wind measurements. To determine which measurements are acceptable and which are intolerably contaminated, the level of contamination must first be assessed.

## III. Contamination Detection Metrics

Each observed $\sigma^o$ value is the sum of the true $\sigma^o$ over the footprint and a noise term

$$\sigma^o_{\text{Obs}} = \sigma^o_{\text{True}} + \eta_o. \tag{1}$$

The true backscatter value ($\sigma^o_{\text{True}}$) for any measurement is the integral of the surface $\sigma^o$ over the spatial response of the antenna [11]

$$\sigma^o_{\text{True}} = \frac{\iint_{A_{\text{slice}}} \sigma^o_{x,y} R_{x,y}\,dxdy}{\iint_{A_{\text{slice}}} R_{x,y}\,dxdy} \tag{2}$$

where $R_{x,y}$ is the spatial response function of the particular slice of interest, $\sigma^o$ is the surface backscatter value, and the bounds of integration are the bounds of the spatial response function.

$\sigma^o_{\text{True}}$ can also be written as the sum of the land and ocean backscatter values separately, as

$$\sigma^o_{\text{True}} = \sigma^o_{\text{Land Contribution}} + \sigma^o_{\text{OceanContribution}} \tag{3}$$

and, in integral form

$$\sigma^o_{\text{True}} = \frac{\iint_{A_{\text{Land}}} \sigma^o_{x,y} R_{x,y}\,dxdy}{\iint_{A_{\text{Slice}}} R_{x,y}\,dxdy} + \frac{\iint_{A_{\text{Ocean}}} \sigma^o_{x,y} R_{x,y}\,dxdy}{\iint_{A_{\text{Slice}}} R_{x,y}\,dxdy} \tag{4}$$

where $A_{\text{land}}$ and $A_{\text{ocean}}$ are the regions of the footprint consisting of land and ocean, respectively.

Land-contaminated $\sigma^o$ values are those where $\sigma^o_{\text{Land Contribution}}$ adversely affects $\sigma^o_{\text{Obs}}$, resulting in a large bias in the wind estimate. The level of contamination can be determined using a number of metrics; however, in this paper, we evaluate only two, namely, MDL and LCR.

### A. MDL

Outside of the 3-dB contour for any slice, the response pattern drops sharply [3]. When the location of the 3-dB contour is greater than a certain distance (typically 30 km) from land, the observed $\sigma^o$ value is not land contaminated. This relationship between land contamination and the 3-dB contour is the basis for the MDL metric. The MDL for each slice is the smallest distance to land from any corner of the 3-dB contour.

Variations of the MDL metric include using the distance to land along the major and minor axes of the slice or in any direction from the slice. A variant of the MDL is used in the conventional Jet Propulsion Laboratory (JPL) processing of QuikSCAT data [12].

### B. LCR

A second metric for detecting land contamination is the LCR. Rather than using distance to the spatial response 3-dB contour similar to that of the MDL, the LCR uses the full spatial response for each slice. The spatial response is used to weight the calculation of how much land contributes to a measurement. The LCR for a measurement is the normalized and weighted integral of the land contributing to the backscatter. To calculate the LCR, we assume that $\sigma^o$ for land is constant. The LCR is then the ratio of $\sigma^o_{\text{Land Contribution}}$ normalized by the $\sigma^o$ of a land-only measurement ($\sigma^o_{\text{Land}}$), which can be written as

$$\text{LCR} = \frac{\sigma^o_{\text{Land Contribution}}}{\sigma^o_{\text{Land}}} = \frac{\iint_{A_{\text{land}}} R_{x,y}\,dxdy}{\iint_{A_{\text{slice}}} R_{x,y}\,dxdy}. \tag{5}$$

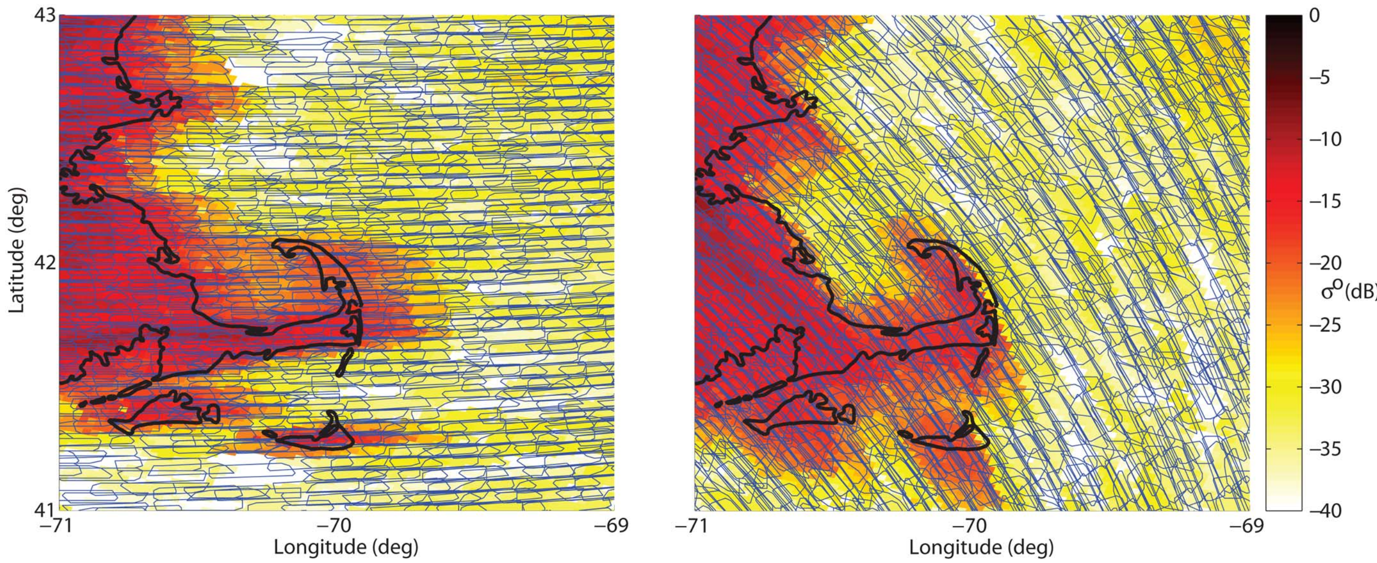


Fig. 2. Cape Cod, Massachusetts, coastline region overlaid with forward- and aft-looking vertically polarized slices and high-resolution $\sigma^o$ in decibels. The $\sigma^o$ values for land in this region are about $-10 \pm 5$ dB, and ocean values are between $-50$ and $-25$ dB. The $\sigma^o$ values above $-25$ and below $-15$ dB are almost certainly land contaminated. Note particularly that the land contamination spreads away from land most significantly in the same general direction as the major axis of the slices.

Rather than using the full continuous response function, in practice, we simplify computation by using a close approximation sampled at a 1-km resolution. This simplified computation is performed using

$$\mathrm{LCR} = \frac{\sum_{x,y} L_{x,y} R_{x,y}}{\sum_{x,y} R_{x,y}} \tag{6}$$

where $x$ and $y$ are in kilometers away from the slice center, $L_{x,y}$ is the land indicator function consisting of a "one" for land and a "zero" for ocean, $R_{x,y}$ is the antenna response, and LCR is the land contribution ratio. The bounds of summation over $x$ and $y$ from the center of the slice can vary depending on the desired accuracy.

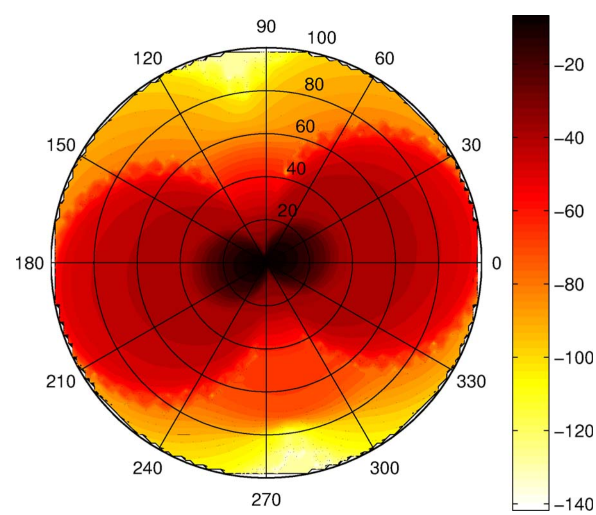


Fig. 3. Contour map of the LCR, in decibels, as a function of the distance in kilometer from the center of the slice to the coastline generated using one slice of the vertical polarization antenna spatial response, as shown in Fig. 1. The angles shown refer to the angle between the slice minor axis and the coastline. Note that the LCR has a high directional dependence.

### *C. Metric Comparisons*

To effectively evaluate the MDL and LCR metrics, both direct and indirect comparisons are used. Initially, a direct comparison is made of the MDL and the LCR. Afterward, the metrics are indirectly compared, first by using the correlation between the metric value and $\sigma^o$. A further comparison is made of the number of $\sigma^o$ measurements each metric deems uncontaminated for an identical coastal region. Although the indirect comparison data plotted throughout this paper are limited to one pass over the Aegean Sea ($38^\circ$ N $\pm 4^\circ$ $25^\circ$ E $\pm 5^\circ$, QuikSCAT rev. 21417), it is representative of other coastal data sets.

To perform a direct comparison between the MDL and LCR metrics, we use a variant of the MDL, where instead of using the shortest distance to the coast from the 3-dB contour, we use the shortest distance to land from the center of the slice. In the comparison, we simulate a straight coastline and then vary the distance to the coast and the orientation of the slice. The LCR, in decibels, is plotted as a function of distance to land and the angle between the minor-axis direction and the coastline, as shown in Fig. 3.

Fig. 3 shows the rapid falloff of the spatial response function in the minor-axis direction. When the minor-axis direction is perpendicular to the coast ($90^\circ$ and $270^\circ$), the LCR is lower than when the major axis is perpendicular to the coastline ($0^\circ$ and $180^\circ$). The significant variation of the LCR with orientation suggests that the distance to land from the slice center alone is not an adequate predictor of land contamination in near-coastal regions. Although there is significant variance in the LCR as a function of direction, as the distance increases to greater than 30 km in any direction, the LCR falls below a level

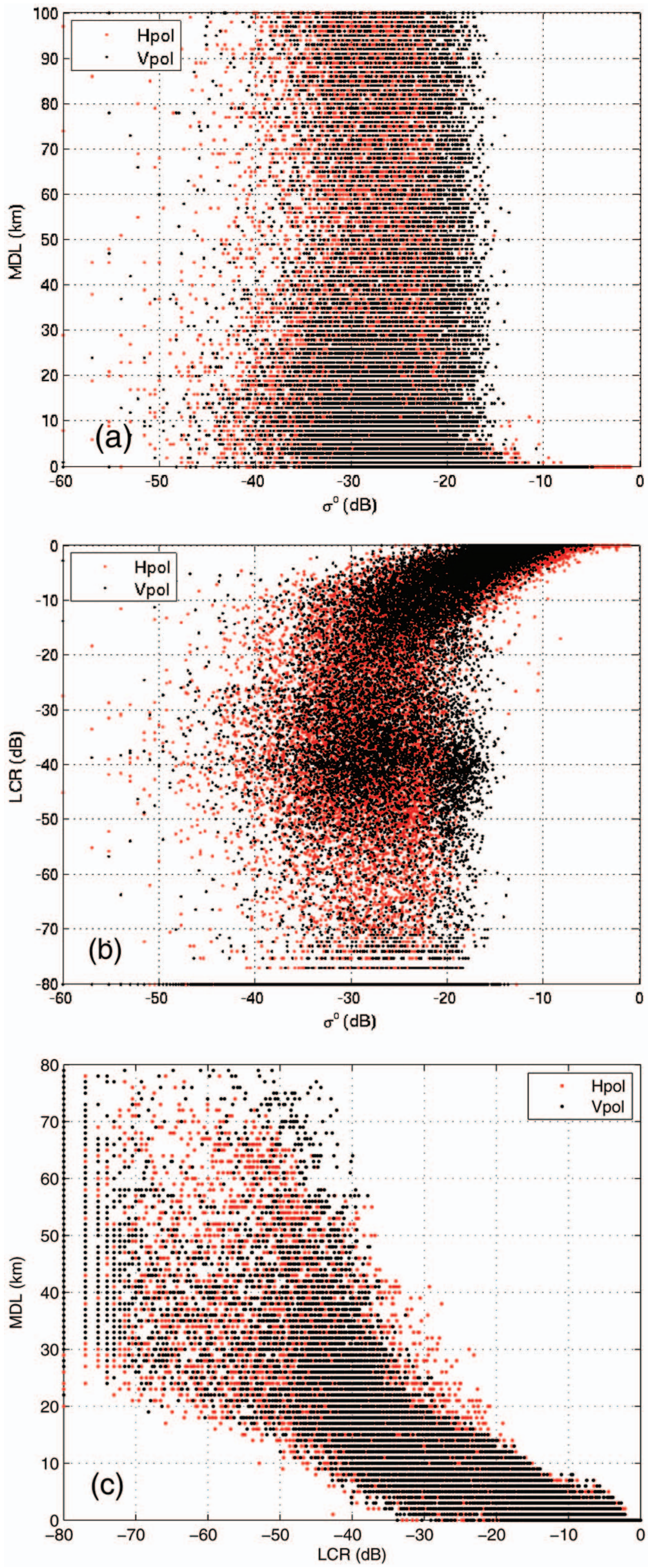


Fig. 4. (a) $\sigma^o$ versus MDL for all polarizations (note that, because the MDL is in 1-km increments, MDL values are quantized to 1 km in the plot). (b) $\sigma^o$ versus LCR, in decibels, for vertical and horizontal polarizations. For plotting, $10^{-8}$ was added to all LCR values so that the ocean $\sigma^o$ values (LCR = 0) can be displayed. (c) LCR versus MDL for a calm coastal area. For plotting, $10^{-8}$ was added to all LCR values (all polarizations).

that affects wind retrieval. This level varies as a function of land brightness and wind speed and will be discussed later. The LCR values shown in Fig. 3 indicate approximately how the LCR behaves in the proximity of a straight coastline. We note that in practice, coastlines are very rarely straight; thus, LCR values can be significantly higher or lower for a given distance to the mean coastline.

The results of the direct comparison between the MDL and the LCR shown in Fig. 3 provide a general idea of the relation between the two metrics. The direct comparison made between the MDL and LCR metrics is limited, however, because the distance to land from the slice center is used rather than the MDL. To compensate, we compare both metrics to the corresponding $\sigma^o$ values and then evaluate the results.

A scatter plot of the $\sigma^o$ value and the MDL for each slice in the test region for the specified orbit is shown in Fig. 4(a). One of the principle limitations of the MDL is that slices which overlap or are next to land have low MDL values, indicating land contamination; nevertheless, some slices are contaminated and some are not. This limitation is particularly apparent in Fig. 4(a), where measurement slices with an MDL of zero spread from $-1$ to $-50$ dB, which includes the range of both land and ocean $\sigma^o$ rather than just one or the other. In order for the MDL to be an ideal metric, as the slices approach land, there should be a gradual transition from the $\sigma^o$ of ocean to the $\sigma^o$ of land. Considering that there is no such transition in Fig. 4(a), it is impossible to quantify the contamination level of slices which lie partially over land.

The corresponding plot of LCR and $\sigma^o$ is shown in Fig. 4(b) for all slices in the region. Note that a smooth rise in backscatter values from the ocean to the land value is readily apparent. Slices that lie entirely over land have LCR values near 0 dB and $\sigma^o$ values which vary closely around $\sigma^o_{\mathrm{Land}}$ for this region, $-10$ dB. Slices entirely over ocean have LCR values close to $-80$ dB and $\sigma^o$ values which vary around $-30$ dB, an expected level for ocean with wind speeds below 10 m/s. Between insignificant land contribution (LCR values below $-30$ dB) and land (0 dB), the backscatter values increase smoothly until they reach $\sigma^o_{\mathrm{Land}}$.

To quantitatively compare the results shown in Fig. 4(a) and (b), the correlation between the metric and $\sigma^o$ is used. The correlation of $\sigma^o$ and the MDL is 44%, while the correlation with $\sigma^o$ for the LCR is 81% when using vertically polarized measurements and 76% when using horizontally polarized measurements. The significantly higher correlation between the LCR and $\sigma^o$ suggests that the LCR offers a more meaningful metric for detecting and removing land contamination. Wind conditions in the study area can have a large effect on the correlation of $\sigma^o$ with either metric. The data shown in Fig. 4(a) and (b) are from a calm ocean, which results in a large distinction between land and ocean backscatter.

The indirect comparisons of the MDL and LCR metrics show that the LCR offers better correlation with measured data and a finer transition between land and ocean, making the LCR a more suitable metric for land-contamination detection. Considering that the transition between land and ocean using the LCR is less abrupt, it allows for the selection of thresholds for a variety of conditions.

### D. Threshold Detection

An LCR threshold can be used to remove land contamination by discarding any $\sigma^o$ values with an LCR greater than a given level. Observe that, in Fig. 4(b), there is a relatively smooth transition of $\sigma^o$ values as the LCR approaches 0 dB. Suppose that an LCR threshold is set at $-20$ dB to remove the section of data where $\sigma^o$ values start to approach the $\sigma^o$ of land. Setting an LCR threshold at $-20$ dB declares all slice measurements below a $-20$-dB LCR to be free of land contamination.

Correspondingly, a threshold using the MDL removes all slices with an MDL below a given level. As an example, an MDL threshold of 20 km indicates that slices in which the MDL is greater than 20 km are not land contaminated.

We compare the number of slice measurements deemed valid by each method in Fig. 4(c), which shows the LCR and MDL for each slice in the region. Setting an LCR threshold at $-20$ dB and discarding all slices with greater contamination levels yield approximately 37 036 valid measurements. A conservative comparison of the LCR to the MDL discards all slices that have LCR values above a certain level and uses the upper MDL value for a given LCR as the smallest MDL allowed. Fig. 4(c) shows that the MDL above which all contamination is below a $-20$-dB LCR is around 15 km. A minimum distance threshold of 15 km in this case yields only 31 844 valid slice measurements from the same data set. If the MDL is used as a metric to identify and remove land contamination, there will be over 5000 slices discarded in coastal regions that are not significantly contaminated. Using the MDL as the land-contamination metric therefore results in larger regions near the coast where no wind can be retrieved.

Fig. 4(c) shows that setting a lower MDL threshold allows slices with significant land contamination, as computed by the LCR, to be declared valid. Fig. 4(c) shows that for the set of slices with a given MDL, there is a large range of LCR levels in the set. The worst case land contamination for a fixed MDL is indicated by the largest LCR in the set. For example, a 30-km MDL threshold removes most land contamination but allows up to a $-24$-dB LCR, while a 10-km MDL threshold allows up to a $-15$-dB LCR. A $-15$-dB LCR level indicates relatively high contamination and results in contaminated wind estimates.

### E. Metric Choice

We can conclude, after comparing both the MDL and LCR land-contamination metrics, that the LCR is a superior metric for land-contamination detection and removal. The LCR correlates better with $\sigma^o$ values, and additionally, the MDL must discard uncontaminated slices to ensure the removal of all contamination, while the LCR retains far more slices for wind retrieval.

However, the fixed LCR threshold used in previous examples is a nonoptimal solution to the land-contamination problem. To optimally identify land-contaminated measurements in all wind conditions, thresholds must change both temporally and spatially with changes in wind speed and land backscatter levels.

## IV. LCR Threshold Determination

Radar backscatter values over the ocean are a function of antenna azimuth, incidence angle, and wind speed. Each factor must be accounted for when setting LCR thresholds.

Depending on the wind speed, QuikSCAT-observed backscatter values over the ocean can be as low as $-50$ dB and as high as $-10$ dB, whereas backscatter values over coastal land regions typically vary between $-15$ and $-5$ dB. The large range of ocean backscatter values causes land contamination in near-coastal regions to have very different effects depending on the local wind speed. When wind speeds are low, even small levels of land contamination can bias wind retrieval enormously. When wind speeds are high, however, a measurement can tolerate much greater land contamination before introducing a significant error during wind retrieval. For land contamination detection, we generate threshold levels using the LCR that are based on localized wind speeds, localized land backscatter and the cross-track location of the measurement.

LCR threshold levels can be understood to be the LCR value for a given slice above which land contamination has significant impact on retrieved wind speeds. Below the threshold, any land contamination has negligible impact. Retrieved wind speeds have a nonlinear relation to backscatter values and are highly susceptible to error from land contamination. To enable the LCR to be an effective land-contamination impact flag, threshold levels are determined via simulation, where both nonlinear effects and biases are taken into account.

Ideally, LCR thresholds would be determined by processing the backscatter values from an observed region with a truth wind field. Considering that appropriate wind data are not readily available, we instead use Monte Carlo-simulated backscatter values from simulated wind fields to calculate the rms speed error and choose appropriate LCR thresholds for coastal wind retrieval.

### A. Compass Simulation

Compass simulation is a historically valuable tool in performing Monte Carlo simulations for wind retrieval [13], [14]. To generate accurate and meaningful thresholds for use in wind retrieval, we use compass simulations of land-contaminated winds. Compass simulations use a variety of wind speeds at all compass directions. Compass simulation for land-contaminated winds also varies the land-contamination levels. To simplify the wind retrieval and to obtain more accurate $\sigma^o_{\mathrm{Ocean}}$ estimates, we use wind fields that are uniform in speed and direction. The QuikSCAT high-resolution wind-retrieval algorithm is used in the simulation. To simultaneously gain insights about error levels in land-contaminated regions and to relate land-contaminated wind errors to the average error across the swath, we choose to apply land contamination to the entire simulated wind field.

### B. Land-Contamination Simulation

Ocean backscatter values $\sigma^o_{\mathrm{Ocean}}$ are created for each slice in the simulation. We then use (7) to generate simulated land-contaminated backscatter values with multiplicative noise

$$\sigma^o_{\mathrm{Obs}} = \sigma^o_{\mathrm{Land}}\mathrm{LCR} + \sigma^o_{\mathrm{Ocean}}(1 - \mathrm{LCR}) + \eta_0 \qquad (7)$$

where $\eta_0$ is a zero-mean Gaussian noise proportional to

$$\sigma^o_{\mathrm{Land}}\mathrm{LCR} + \sigma^o_{\mathrm{Ocean}}(1 - \mathrm{LCR}).$$

Both LCR and $\sigma^o_{\mathrm{Land}}$ are constant for each simulation.

Rather than placing land regions in the wind field and calculating the LCR for each slice, we fix the LCR and $\sigma^o_{\mathrm{Land}}$ for an entire wind field. Fixed levels are advantageous in that they cause all slice measurements to be uniformly contaminated. Uniform contamination of slice measurements would be otherwise impossible due to the shape of the antenna response pattern and the irregular sampling pattern of the scatterometer. For each LCR and $\sigma^o_{\mathrm{Land}}$ realization, there are 114 000 total WVCs in each simulated wind field and 1500 WVCs per cross-track index, which are used to calculate the land-contamination errors.

After generating the land-contaminated backscatter measurements from the true wind fields, wind retrieval is performed using the simulated backscatter values and the GMF. To minimize additional errors caused by ambiguity selection, the nearest ambiguity to the simulated wind is chosen in all cases.

### C. Simulation Results

After wind retrieval and ambiguity selection, error levels are calculated for each simulated wind field. The rms wind-speed error, in meters per second, is calculated for each cross-track location using the difference between the retrieved and true winds for each WVC in the cross-track direction. The rms wind-speed error requirements are defined in the QuikSCAT mission objectives to be 2 m/s for wind speeds from 2 to 20 m/s and 10% for wind speeds from 20 to 30 m/s [12].

The QuikSCAT scatterometer has different instrument-skill levels as a function of the cross-track swath location—error levels vary based on the instrument skill. Instrument skill relates mainly to the azimuthal diversity achieved for any cross-track swath location. Cross-track locations near the nadir track and at the far swath have much less azimuthal diversity than do midside swath WVCs; hence, the instrument skill is lower, and the cells generally have greater error levels. Fig. 5 shows the error levels without land contamination for each cross-track bin for each simulated wind speed and illustrates the necessity of different error levels for each cross-track bin due to the instrument skill.

Although excessive levels of land contamination cause errors in the retrieved wind speed, some error is tolerable. Thus, for each cross-track index, we choose acceptable rms error levels that are a percentage of the true wind speed. Choosing acceptable error levels as a function of the cross-track index allows any additional error due to land contamination to vary together with the instrument skill.

Fig. 6 shows a contour plot of the rms error, in meters per second, as a function of wind speed and LCR level for one wind direction, one land-reflectivity level, and one cross-track WVC. The rms error-level contours illustrate how susceptible

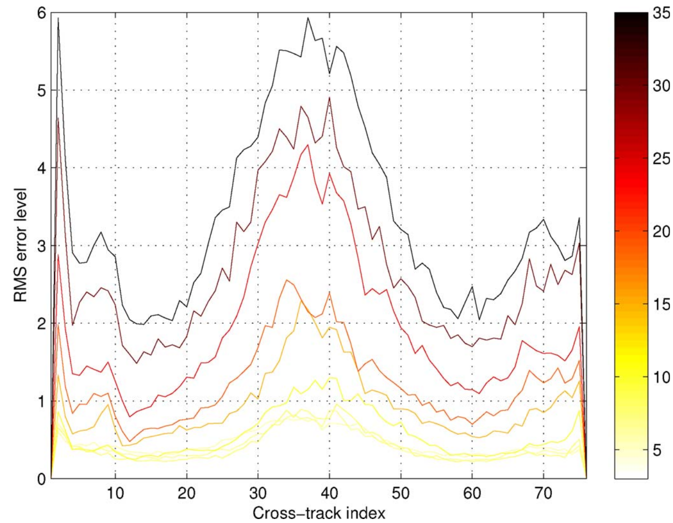


Fig. 5. RMS error levels, in meters per second, as a function of the cross-track WVC for each of the simulated wind speeds, in meters per second, without land contamination. The color scale indicates wind speed. Wind speeds are in ascending order, bottom to top. Nadir is at the cross-track index 38.

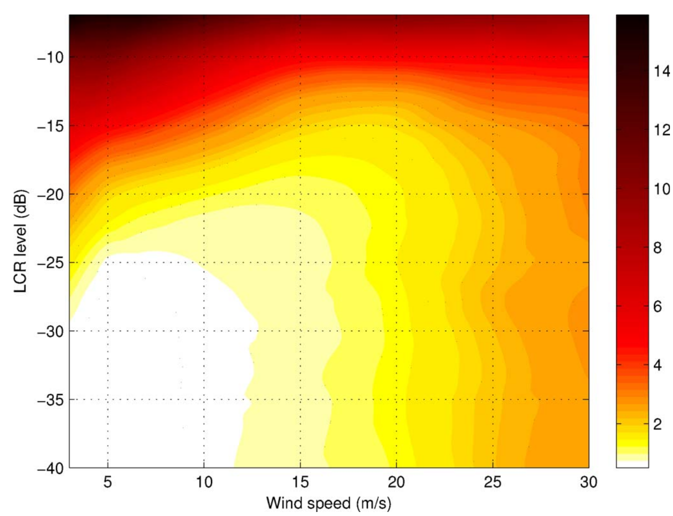


Fig. 6. RMS error contours in meters per second from the rms error surface as a function of the simulated wind speed and the simulated LCR level for a single wind direction and land-reflectivity level.

the wind is to land contamination at various wind speeds. For wind speeds above 20 m/s, the error levels, as a function of land contamination, are roughly the same until the LCR values reach about $-10$ dB, which illustrates how higher wind speeds are tolerant of land contamination. Lower wind speeds, particularly those below 10 m/s, are intolerant of land contamination with LCR values above $-20$ dB.

Fig. 7 shows the simulation rms speed error, in meters per second, as a function of wind speed for each of the simulated directions without land contamination. As expected, the error levels for different directions are roughly similar except when winds are near parallel to the along-track direction. Considering that there is relatively little variation in the wind-speed error due to wind direction, we choose to eliminate wind direction as a variable in threshold determination. Instead, to determine the LCR thresholds, we choose the worst case wind direction for each cross-track WVC.

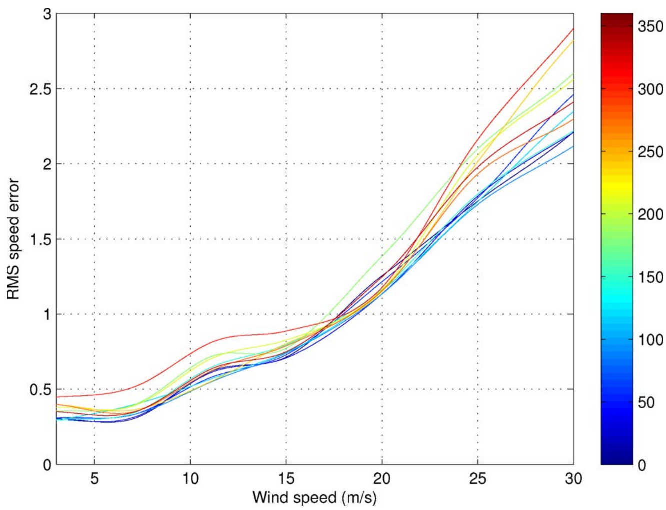


Fig. 7. RMS wind-speed error in meters per second without land contamination for compass directions spaced every 30° in the central cross-track region (cross-track WVC 27). Error lines with slightly higher error levels correspond to winds in the along-track direction. The color scale indicates wind direction.

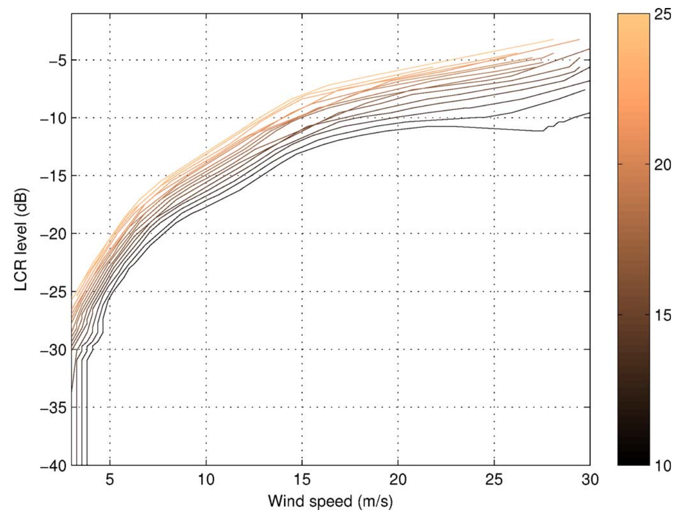


Fig. 8. LCR threshold levels as a function of wind speed for 10%–25% RMS wind-speed error for cross-track WVC 20. Lines are spaced every 1%, and the line color indicates the specific rms speed error level in percent. Thresholds for lower error levels are closer to the bottom of the figure.

The rms wind-speed error from the simulated wind fields suggest that the dominant variables in determining LCR thresholds are wind speed, cross-track location, and land brightness levels. We use these variables simultaneously to choose the LCR threshold levels.

Selecting an appropriate LCR threshold for each cross-track location involves several steps. For each cross-track WVC and land reflectivity, we first find the wind direction that causes the worst rms wind-speed error without land contamination. Second, using the worst case wind direction, we determine the rms wind-speed error as a function of wind speed and LCR. Third, we find the maximum LCR value for each wind speed for which the rms wind-speed error is below a percentage of the wind speed. The maximum LCR value becomes the LCR threshold for that wind speed. The percentage of the wind speed associated with the LCR threshold is different for each WVC, to reflect the differences in instrument skill across the swath. This percentage of the wind speed is the tolerable rms speed error level for that WVC.

The tolerable rms speed error level for each cross-track WVC is chosen by finding an error level that is achievable for low wind speeds and sufficiently smooth for high speeds. If the tolerable error level is set too low, the specified error level cannot be met for low wind speeds. For high wind speeds, we stipulate that the LCR thresholds resulting from the specified error level must be smooth as the wind speed increases.

Fig. 8 shows the LCR threshold levels resulting from illustrative rms wind-speed errors for 10%–25% of wind speed for a fixed land reflectivity and cross-track WVC. If error levels are set below 13% of the wind speed, it is impossible to meet the criteria for the lowest wind speeds, even with relatively little land contamination. Conservative rms speed error levels can be subjectively chosen between 14% and 20% for each WVC. Such a conservative rms speed error level is chosen to effectively maximize the number of retrievable WVCs while maintaining good wind estimation.

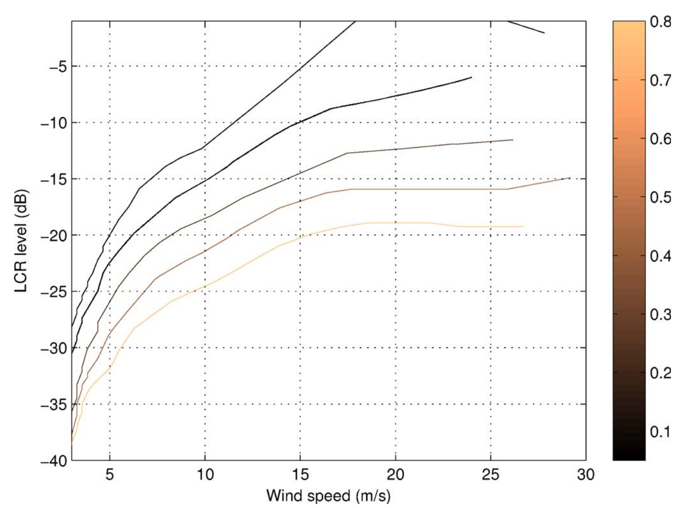


Fig. 9. LCR threshold levels as a function of wind speed for varying land-reflectivity levels with 15% rms wind-speed error for cross-track WVC 20. Line color indicates the land-reflectivity levels. Thresholds for lower land-reflectivity levels are near the top of the figure.

After determining the LCR threshold for each cross-track WVC, we observe that the average of the selected error levels for the entire swath is 18%. The average error level of 18% is lower than the QuikSCAT mission specifications for low wind speeds and slightly higher for high wind speeds.

When the error level from Fig. 8 is fixed at 15% of wind speed and the land brightness is varied in simulation, Fig. 9 shows the necessary LCR thresholds as a function of the wind speed for the same cross-track WVC.

As shown in Fig. 9, land-reflectivity levels affect the LCR threshold levels significantly; hence, it is important to obtain accurate estimates for the land brightness. Practical experience with scatterometer data and land contamination shows that the land brightness is quite different for each polarization and look (fore and aft).

The temporal and spatial variability of land brightness requires land-reflectivity estimates that are accurate, both temporally and spatially, for each polarization and look. The spatial accuracy of the land brightness estimates depends somewhat on the accuracy of the reported slice location and the land map. The QuikSCAT measurement locations have a 2.5-km location accuracy. The land map used to estimate the LCR and land brightness has a 1-km accuracy. The LCR thresholds set in simulation and the mechanisms used to obtain temporal estimates minimize the effects of location errors. The method we use to obtain temporally accurate estimates is explained later.

To effectively utilize the LCR thresholds determined in simulation, the thresholds are tabulated in a lookup table. Thresholds are indexed according to the local wind speed, cross-track index, and local land reflectivity. Local LCR thresholds are then set during AVE processing so that contaminated measurements are discarded prior to performing wind retrieval. Although LCR processing is performed independently from wind retrieval, to evaluate the success of the LCR algorithm, we must evaluate the wind-retrieval results.

## V. Wind Retrieval

The LCR algorithm is implemented as a part of the AVE resolution-enhancement algorithm to produce high-resolution (2.5 km) $\sigma^o$ fields for use in high-resolution wind retrieval that are free of land contamination. The LCR algorithm can also be used for conventional (25 km) wind products. This section compares both the conventional and high-resolution standard wind products with their LCR-processed counterparts.

Previous wind-retrieval methods avoid land contamination by using distance thresholds similar to the MDL, resulting in large areas where no wind estimates can be made, rather than determining the impact of land contamination on every measurement, as is done with the LCR method. The 25-km low-resolution QuikSCAT product produced by JPL, known as L2B, uses a distance threshold of 30 km from the coast within which all measurements are discarded. Fig. 10 shows the 25-km WVCs from the L2B data product file for one pass. Although a 30-km threshold effectively removes all land contamination, the regions without wind estimates are larger than necessary.

High-resolution wind retrieval is advantageous in that it can be performed on a 2.5-km grid up to the coastline. This method is useful, as it often retrieves valid winds closer to the coast than possible with low-resolution wind retrieval; however, due to land contamination, wind speeds next to the coast are often inaccurate, producing wind-speed errors of up to 20 m/s.

Fig. 11 shows high-resolution winds retrieved from $\sigma^o$ fields created using the AVE algorithm. Land-contaminated winds are readily apparent in Fig. 11 as very high wind speeds near the coast. Note that land-contaminated winds do not spread out from land uniformly in all directions due to the varying aspect angles of the antenna response pattern sidelobes over the swath, as shown in Fig. 2.

To compensate for land contamination in high-resolution wind fields, previous methods have used a 30-km distance threshold as in the low-resolution L2B wind products discussed previously. Fig. 12 shows that a 30-km distance threshold effectively removes land contamination in high-resolution wind fields. Unfortunately, the conservative threshold removes a large number of potentially valid WVCs, resulting in large gaps where wind retrieval could be possible. In this example, there are 53 527 fewer WVCs with wind estimates using a 30-km threshold rather than standard high-resolution wind retrieval. Note that there are several places where apparently reasonable wind estimates in Fig. 11 are discarded in Fig. 12, such as in the northern region of the Aegean Sea.

### A. Wind Retrieval Using the LCR

The LCR metric is designed to identify significantly contaminated $\sigma^o$ measurements so that they can be removed before processing and all uncontaminated winds can be retrieved successfully. When contaminated $\sigma^o$ measurements are removed without discarding usable data, the maximum number of accurate uncontaminated wind vectors are retrieved.

Estimates of the local wind speeds are obtained during processing from the JPL L2B 25-km-resolution product for the corresponding orbit. Considering that LCR thresholds change significantly as a function of wind speed, conservatively accurate wind estimates are maintained by setting wind-speed-dependent LCR thresholds using the minimum wind speed in the local area. The local wind-speed estimate is the minimum wind speed in a $5 \times 5$ along-track by cross-track WVC area according to the L2B file. L2B wind-speed estimates are ideal for setting LCR thresholds because L2B wind estimates are generated only for WVCs where there is no significant land contamination. LCR thresholds set according to L2B wind speeds are therefore unbiased by the land contamination. One drawback of using L2B wind speeds is that, because they use large distances to avoid land contamination, the L2B wind estimates are sparse and there are areas where there are no L2B estimates in the $5 \times 5$ WVC surrounding area. To compensate, if no L2B wind speeds are found within a $5 \times 5$ WVC area, a $9 \times 9$ WVC region is searched. If there are no L2B estimates in a $9 \times 9$ WVC area, a default threshold is used.

To set the LCR thresholds appropriate to the local region, the land backscatter is estimated prior to wind retrieval. Land backscatter is nonisotropic, particularly in mountainous regions where the true incidence angle of the antenna beam can vary greatly. To compensate for the directional dependence of backscatter values, the maximum $\sigma^o$ value for each antenna beam in a local-area region is used to set LCR thresholds. Each look has a separate land-reflectivity estimate. To obtain temporal resolution of land reflectivity, an array of maximum backscatter values is created using the current orbit data for each look prior to LCR processing. LCR thresholds are then set based on the maximum backscatter values in a $3 \times 3$ along-track by cross-track region according to the worst case backscatter estimates for each look.

Once LCR thresholds are set, land-contaminated slices are discarded, and uncontaminated $\sigma^o$ fields are created at both conventional and high resolution. To create low-resolution $\sigma^o$ measurements, the retained slices are averaged by polarization and look direction for each WVC. Wind retrieval is then performed, creating a low-resolution WVC wind product, as shown in Fig. 13, that is comparable to the L2B winds.

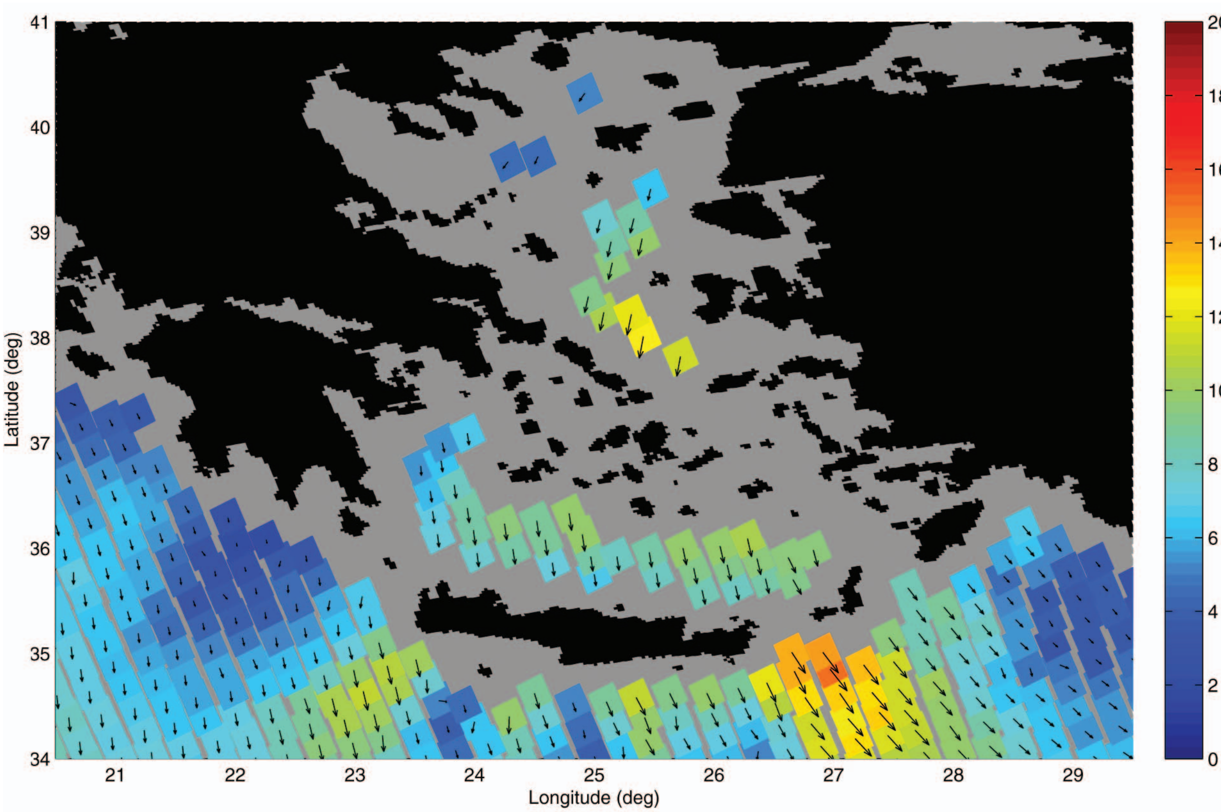


Fig. 10. L2B conventional resolution (25 km) wind speed (in meters per second) and direction wind product. The conservative distance threshold to remove land contamination causes WVCs to be particularly sparse in the region.

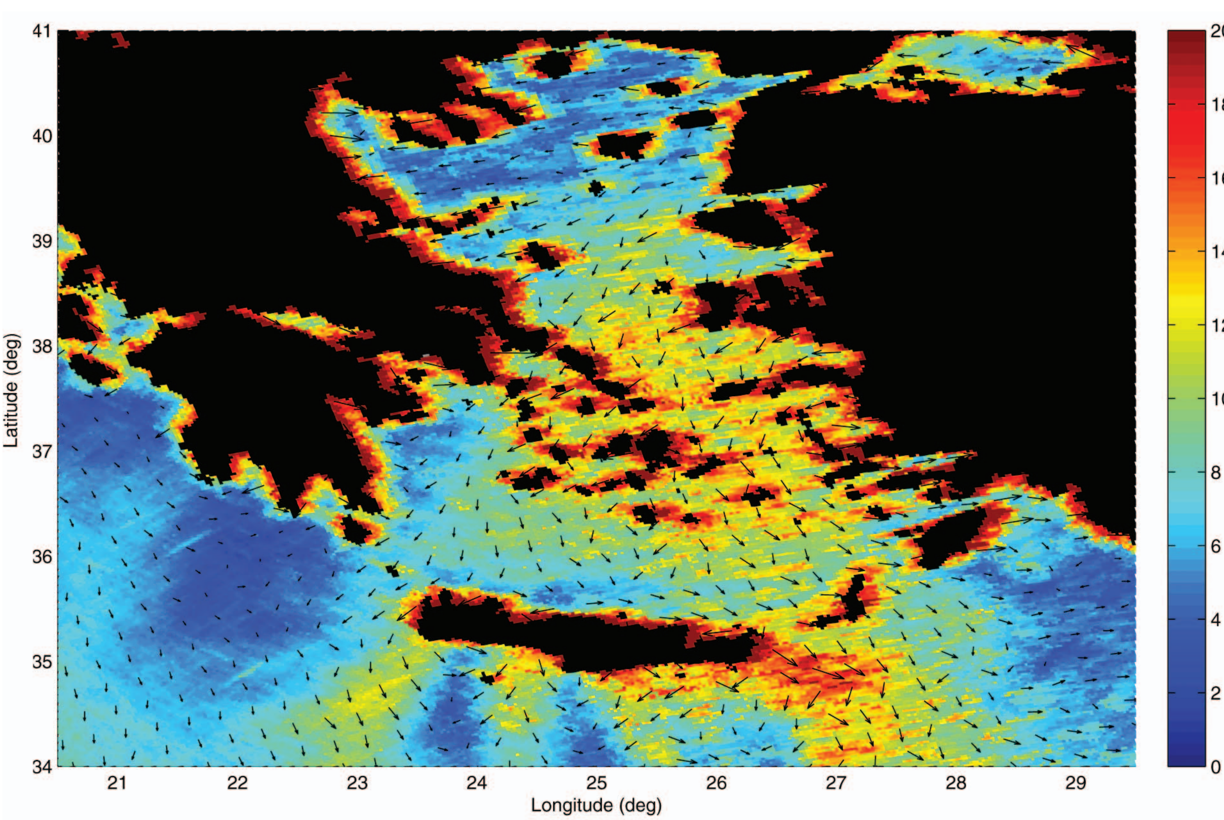


Fig. 11. Wind speed (in meters per second) with wind-direction vectors as retrieved using the high-resolution wind-retrieval algorithm directly for the Aegean Sea. Land-contaminated winds are visually apparent as wind speeds near land of roughly 15 m/s or more.

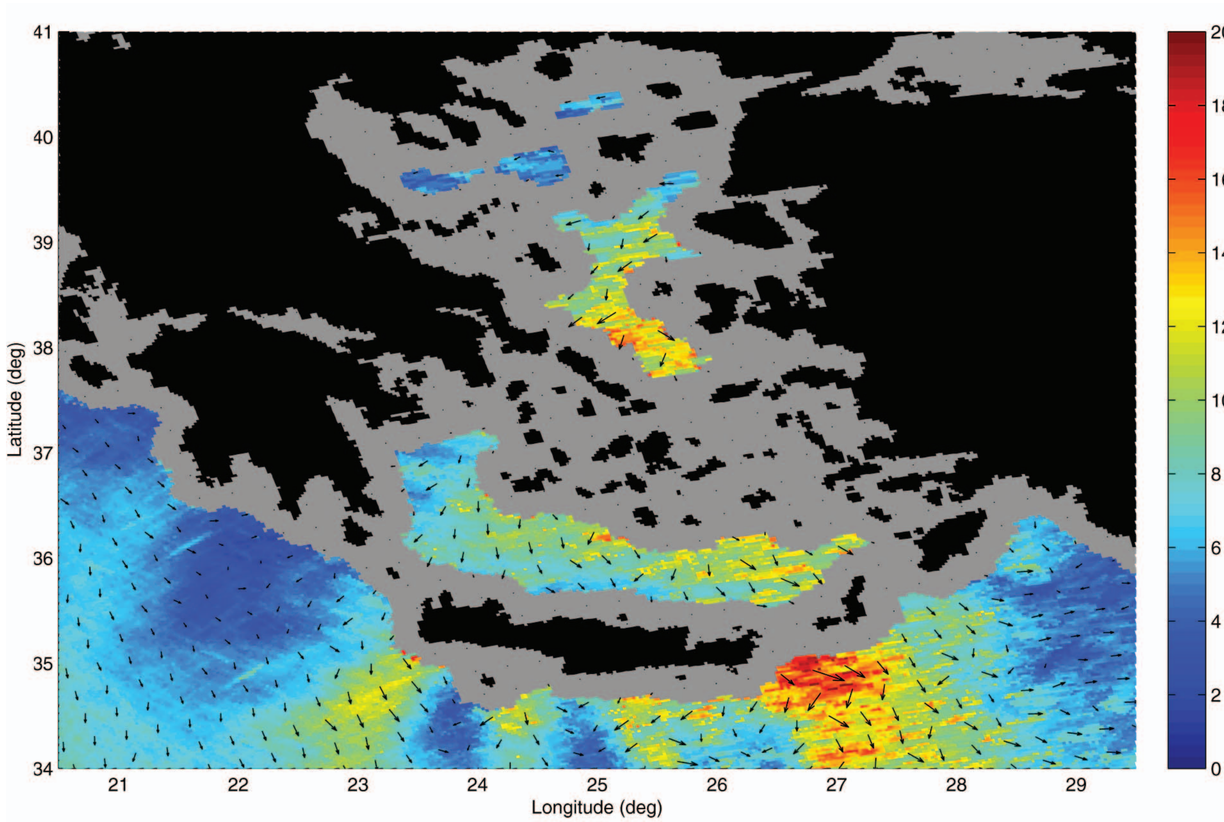


Fig. 12. High-resolution wind speed (in meters per second) and direction produced by discarding all slices within 30 km of the coast. Note the large gaps where wind cannot be retrieved.

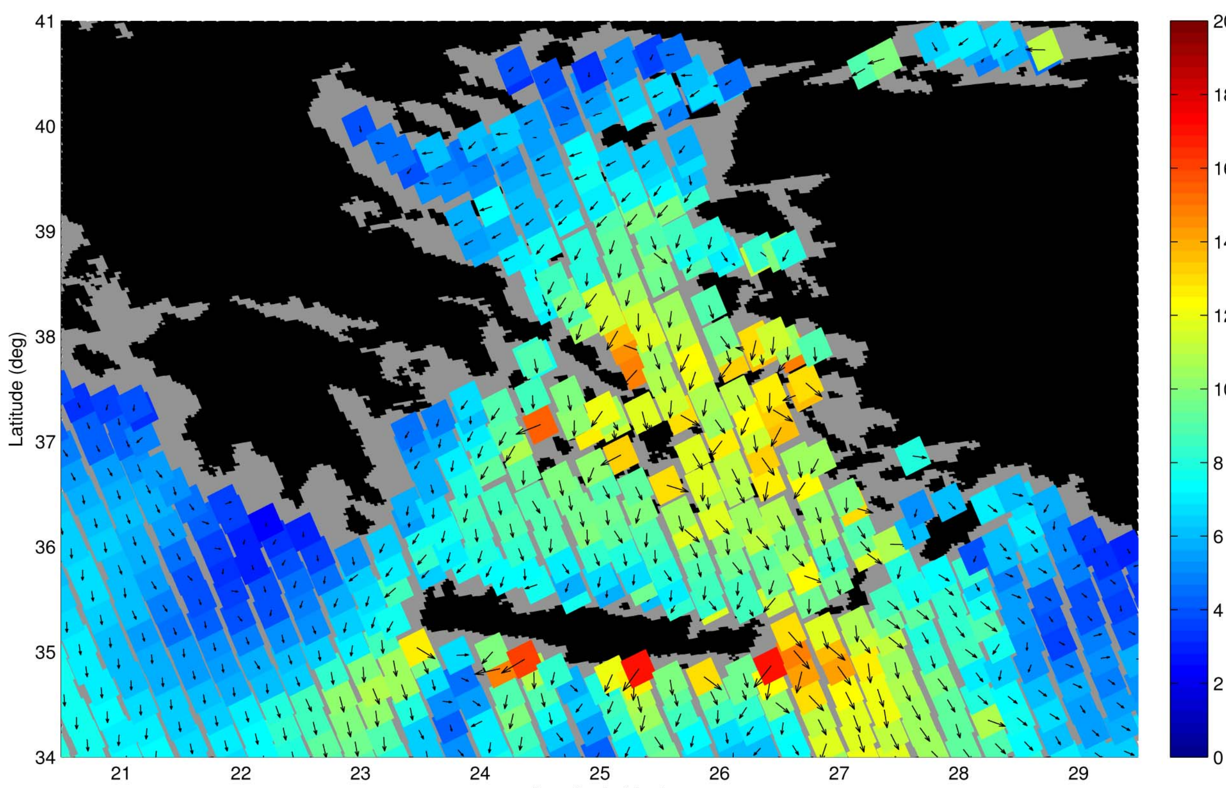


Fig. 13. Conventional resolution wind speed (in meters per second) and direction produced after land-contaminated measurements are discarded. Compare with Fig. 10. Note that WVCs are closer to the coast. The irregular spacing of the WVCs is a consequence of averaging the latitude and longitudes of all slices in each cell.

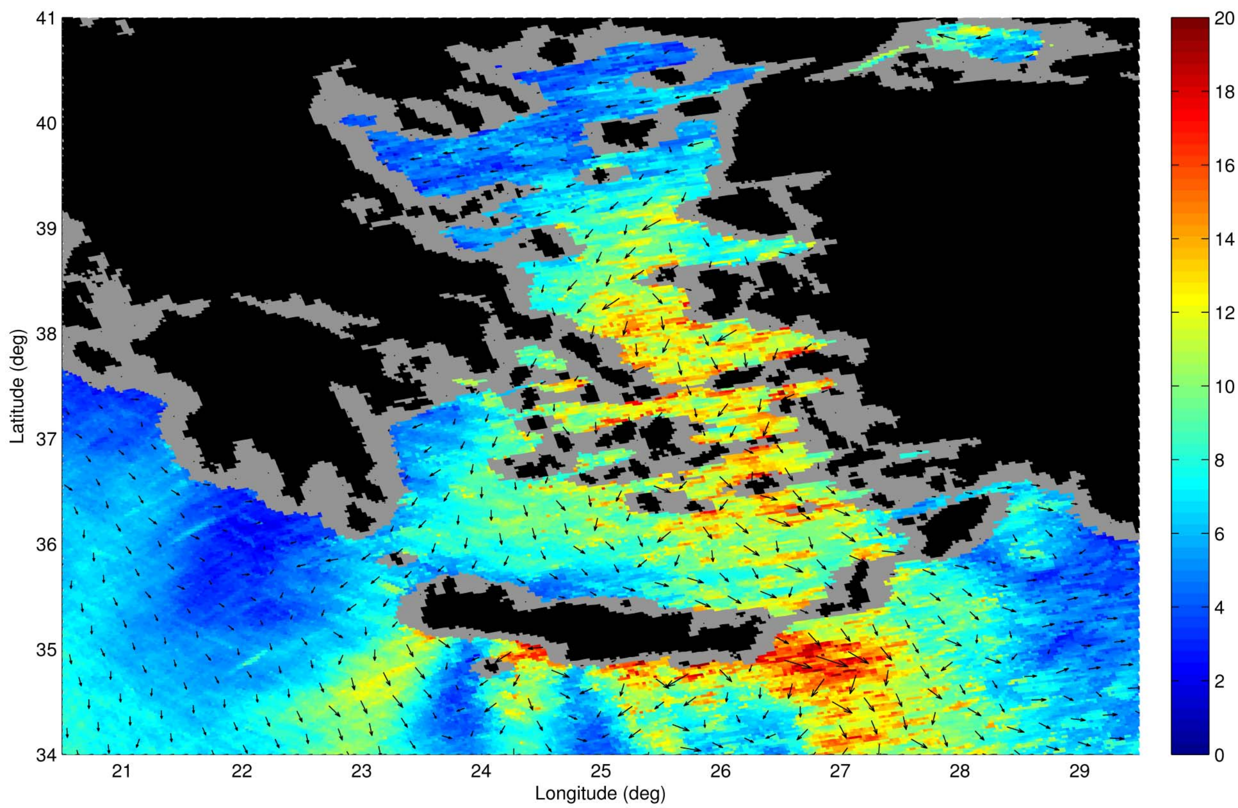


Fig. 14. High-resolution wind speed (in meters per second) and direction retrieved using high-resolution methods after removing land-contaminated slices using the LCR metric.

Several differences are readily apparent between Figs. 10 and 13. The most notable one is the greater number of WVCs with wind estimates in the LCR-processed wind fields which are visually uncontaminated. The greater number of WVCs is a consequence of removing only the slices which are land contaminated instead of those which are within 30 km of land. Not only are there more WVCs in the low-resolution wind field but the additional WVCs are typically much closer to the coastline than any WVC from the L2B data. Unfortunately, averaging slices to simulate pulses has two undesirable consequences. First, when land-contaminated measurements are discarded, fewer measurements remain in each WVC, and wind estimates in near-coastal WVCs are noisier. This may alter the wind-retrieval error distribution. Second, WVCs are no longer as regularly spaced as in L2B winds, as WVC centers are calculated to be the average location of the measurements that they contain. Despite the drawbacks of the pulse approximation, the advantages of LCR processing in low-resolution wind retrieval are still readily apparent.

High-resolution wind retrieval emphasizes the advantages of land-contamination detection and removal using the LCR without the drawback of irregular WVC spacing. Fig. 14 shows high-resolution wind speed retrieved after the LCR processing of backscatter values for the same orbit as Fig. 11. Comparing Fig. 14 with Figs. 11 and 12, it is apparent that LCR-processed winds show the best features of both previous methods. Using LCR processing, it is possible to retrieve wind speeds much closer to the coast than those retrieved using a 30-km threshold. Consequently, wind speeds that appear reasonable in Fig. 11 but are not retrieved in Fig. 12, such as in the northern Aegean Sea, can be retrieved using the LCR. In addition to the accurate portrayal of mesoscale coastal wind features, in this example, the LCR threshold only discards 31 053 high-resolution WVCs, which is a 42% improvement over the number of high-resolution WVCs discarded using the 30-km threshold.

To validate the performance of the LCR over a much larger data set, we compare the distribution of high-resolution wind speeds for one year of QuikSCAT data. We use wind data from a region on the Atlantic coast of the United States ($43^\circ$ N $\pm 2.5^\circ$ $68^\circ$ W $\pm 2.5^\circ$) during 2006. Fig. 15 shows the wind-speed distribution for four subsets of the 2006 data set. The four distributions we compare consist of the following:

1) WVCs greater than 30 km from land;
2) WVCs less than 30 km from land processed using the LCR;
3) WVCs less than 30 km from land processed without the LCR;
4) WVCs processed without the LCR for which LCR processing did not provide a wind estimate.

The distribution of data set 1) consists of uncontaminated winds and thus estimates the true wind distribution. The distribution of near-coastal winds after LCR processing [data set 2)] closely resembles the true wind distribution. This indicates that any land contamination is successfully mitigated using the LCR. We expect the LCR-processed distribution to resemble the ocean wind distribution; however, there may be

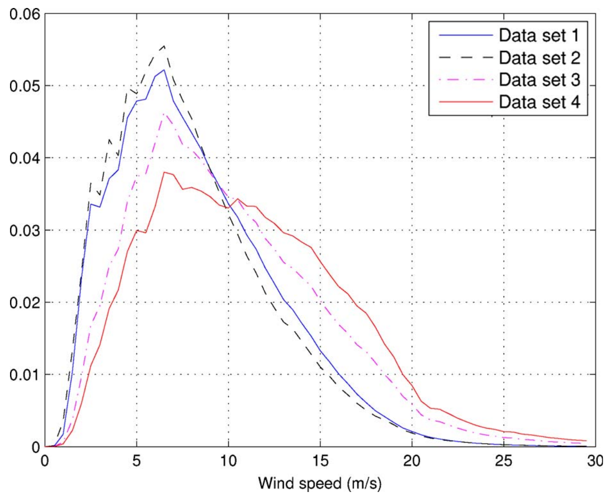


Fig. 15. Wind-speed distributions of the Cape Cod region using all QuikSCAT high-resolution data from 2006. The four different distributions consist of the following: 1) wind speed > 30 km from the coast; 2) LCR-processed wind speed < 30 km from the coast; 3) wind speed < 30 km from the coast; and 4) coastal WVCs where LCR reported land contamination. There are over 160 million WVCs in the combined data sets.

small differences due to coastal wind features, such as coastal jets and lees, not in data set 1).

Comparing the near-coastal winds from data sets 2) and 3), it is easy to see the bias toward higher wind speeds, which occurs as a result of land contamination. To further illustrate the bias caused by land contamination, data set 4) shows the distribution of speeds of WVCs, which the LCR reported as land contaminated. Data set 4) is thus almost purely land contaminated. The increased bias over the distribution of data set 3) is readily apparent. The difference between data sets 3) and 4) further illustrates the success of LCR processing.

## VI. Conclusion

In summary, although the MDL functions as a land-contamination indicator, it is an insufficient metric for use in land-contamination detection and removal. Instead, the LCR, when used with thresholds developed using compass simulation, is a more powerful metric for land-contamination detection. Wind-retrieval results using the LCR show that mesoscale coastal wind features, such as lees and jets, can be accurately portrayed, in addition to a large increase in the number of valid WVCs using both conventional and high-resolution wind retrieval. Wind fields obtained after LCR processing are more accurate and closer to the coast by as much as 25 km than those retrieved using previous methods. This improved ability to retrieve coastal winds increases the utility of the QuikSCAT scatterometer, making large-scale coastal wind studies feasible, which were previously too costly to attempt.

## References

[1] W. Tang, T. Liu, and B. Stiles, "Evaluation of high-resolution ocean surface vector winds measured by QuikSCAT scatterometer in coastal regions," *IEEE Trans. Geosci. Remote Sens.*, vol. 42, no. 8, pp. 1762–1769, Aug. 2004.

[2] D. Long, "High resolution wind retrieval from SeaWinds," in *Proc. Int. Geosci. Remote Sens. Symp.*, Toronto, ON, Canada, Jun. 24–28, 2002, pp. 751–753.

[3] I. Ashcraft and D. Long, "The spatial response function of SeaWinds backscatter measurements," in *Proc. SPIE Earth Observ. Syst. VIII*, W. L. Barnes, Ed., Aug. 3–6, 2003, vol. 5151, pp. 609–618.

[4] D. S. Early and D. G. Long, "Image reconstruction and enhanced resolution imaging from irregular samples," *IEEE Trans. Geosci. Remote Sens.*, vol. 39, no. 2, pp. 291–302, Feb. 2001.

[5] M. Spencer, C. Wu, and D. G. Long, "Improved resolution backscatter measurements with the SeaWinds pencil-beam scatterometer," *IEEE Trans. Geosci. Remote Sens.*, vol. 38, no. 1, pp. 89–104, Jan. 2000.

[6] D. G. Long, J. B. Luke, and W. Plant, "Ultra high resolution wind retrieval from SeaWinds," in *Proc. IGARSS*, 2003, pp. 1264–1266.

[7] D. G. Long, P. J. Hardin, and P. T. Whiting, "Resolution enhancement of spaceborne scatterometer data," *IEEE Trans. Geosci. Remote Sens.*, vol. 31, no. 3, pp. 700–775, May 1993.

[8] M. H. Freilich and R. S. Dunbar, "Derivation of satellite wind model functions using operational surface wind analyses: An altimeter example," *J. Geophys. Res.*, vol. 98, no. C8, pp. 14 633–14 649, Aug. 1993.

[9] F. M. Naderi, M. H. Freilich, and D. G. Long, "Spaceborne radar measurement of wind velocity over the ocean—An overview of the NSCAT scaterometer system," *Proc. IEEE*, vol. 76, no. 6, pp. 850–866, Jun. 1991.

[10] R. Kennett and F. Li, "Seasat over-land scatterometer data. I. Global overview of the Ku-band backscatter coefficients," *IEEE Trans. Geosci. Remote Sens.*, vol. 27, no. 5, pp. 592–605, Sep. 1989.

[11] I. Ashcraft, D. Long, A. Anderson, S. Richards, M. Spencer, and B. Jones, "Sigma-0 retrieval from the SeaWinds on QuikSCAT," in *Proc. SPIE Earth Observ. Syst. IV*, W. L. Barnes, Ed., Denver, CO, Jul. 19–20, 1999, vol. 3750, pp. 171–178.

[12] *SeaWinds on ADEOS-II Level 2B Ocean Wind Vectors in 25 km Swath*, D-24902 ed. Pasadena, CA: Phys. Oceanography DAAC, Jet Propulsion Lab., Oct. 2002.

[13] C.-Y. Chi and F. K. Li, "A comparative study of several wind estimation algorithms for spaceborne scatterometers," *IEEE Trans. Geosci. Remote Sens.*, vol. 26, no. 2, pp. 115–121, Mar. 1988.

[14] T. E. Oliphant and D. G. Long, "Accuracy of scatterometer-derived winds using the Cramér–Rao bound," *IEEE Trans. Geosci. Remote Sens.*, vol. 37, no. 6, pp. 2642–2652, Nov. 1999.

**Michael P. Owen** received the B.S. degree in electrical engineering from Brigham Young University (BYU), Provo, UT, in 2007, where he is currently working toward the Ph.D. degree in electrical engineering in the Microwave Earth Remote Sensing Laboratory, Electrical and Computer Engineering Department.

His current research interests include rain modeling and simultaneous wind and rain estimation at ultrahigh resolution for the QuikSCAT scatterometer.

**David G. Long** (S'80–SM'98–F'07) received the Ph.D. degree in electrical engineering from the University of Southern California, Los Angeles, in 1989.

From 1983 to 1990, he was with the Jet Propulsion Laboratory (JPL), NASA, where he developed advanced radar remote sensing systems. While at JPL, he was the Project Engineer of the NASA Scatterometer (NSCAT) project which flew from 1996 to 1997 and he also managed the SCANSCAT project, the precursor to SeaWinds, which was launched in 1999 and 2002. He is currently a Professor with the Microwave Earth Remote Sensing Laboratory, Electrical and Computer Engineering Department, Brigham Young University (BYU), Provo, UT, where he teaches upper division and graduate courses in communications, microwave remote sensing, radar, and signal processing and is the director of the BYU Center for Remote Sensing. He is the Principle Investigator on several NASA-sponsored research projects in remote sensing. His research interests include microwave remote sensing, radar theory, space-based sensing, estimation theory, signal processing, and mesoscale atmospheric dynamics.

Dr. Long was the recipient of the NASA Certificate of Recognition several times. He is an Associate Editor for the IEEE Geoscience and Remote Sensing Letters.